jmr&t
Journal of Materials Research and Technology
www.jmrt.com.br

Original article

New insight on the solidification path of an alloy 625 weld overlay

Cleiton Carvalho Silva[a,*], *Hélio Cordeiro de Miranda*[a], *Marcelo Ferreira Motta*[a], *Jesualdo Pereira Farias*[a], *Conrado Ramos Moreira Afonso*[b], *Antonio Jose Ramirez*[c]

[a] *Department of Materials and Metallurgical Engineering, Welding Engineering Laboratory (ENGESOLDA), Universidade Federal do Ceará, Fortaleza, CE, Brazil*
[b] *Department of Materials Engineering, Universidade Federal de São Carlos, São Carlos, SP, Brazil*
[c] *Electron Microscopy Laboratory, Brazilian Synchrotron Light Laboratory - CNPEM/ABTLuS, Campinas, SP, Brazil*

ARTICLE INFO

Article history:
Received 1 December 2012
Accepted 16 February 2013
Available online 3 August 2013

Keywords:
Superalloy
Welding
Microstructure
Overlay
625 alloy

ABSTRACT

Ni-based alloys are a special class of engineering material with excellent corrosion resistance in harsh environments. However, microstructural changes due to the solidification, may result in solidification cracks and reduction in the corrosion resistance. Knowing the microchemical and microstructural evolutions during the solidification of these alloys is essential for the understanding of the relationship between the metallurgical aspects and the properties. This research presents a new insight on the solidification path of alloy 625 weld metals deposited by the TIG cold wire process on the C–Mn steel plates. After the welding, samples having been extracted and evaluated by the scanning electron microscope, transmission electron microscopy and energy dispersive X-ray spectroscopy techniques. The results showed the presence of two types of secondary phases, identified as Laves phase and complex nitride/carbide particles. Due to the presence of nitrides particles, stable in the solid state during the melting of the alloy, during the solidification it is noted the occurrence of a complex nitride/carbide precipitation. This implies in a new route to explain the solidification of the aforementioned alloy.

1. Introduction

Nickel based superalloys are an important class of engineering material, due to their excellent combination of corrosion resistance and mechanical properties, including high temperature applications [1]. In this context, the alloy Inconel® 625 stands out as one of the leading commercial Ni–Cr–Mo–Nb alloy grade [2]. Its development in the year of 1964, was designed to meet the market of alloys for high temperature service, however, with the discovery of its exceptional corrosion resistance, it also came to occupy a prominent position in other applications, where corrosion resistance is essential [3].

Nevertheless, its high cost makes it unfeasible in relation to applications in some situations. In order to overcome this obstacle and make it attractive to the manufacturing of

* *Corresponding author.*
E-mail: cleiton@metalmat.ufc.br (C.C. Silva).
2238-7854 http://dx.doi.org/10.1016/j.jmrt.2013.02.008

Table 1 – Chemical composition of the filler metal and base metal.

Item	Chemical composition (wt%)							
	Ni	C	Cr	Mo	Nb	Fe	Ti	Si
AWS ERNiCrMo-3 (INCONEL 625®)	64.43	0.011	22.2	9.13	3.53	0.19	0.23	0.05

Item	Chemical composition (wt%)							
	Ni	C	Cr	Mo	Fe	Al	Mn	Si
ASTM A516 Gr.60	0.01	0.15	0.02	0.01	98.64	0.02	0.95	0.20

equipment, providing high performance in the service with the use of this particular alloy, the deposition of dissimilar welding overlays with Ni-based alloys on C–Mn and low alloy steels, has become a great option in recent years [4]. However, due to the dissimilarity among the metals to be joined and the welding conditions being applied, changes in the chemical composition as an enrichment of the Ni-based alloy by Fe and C, due to the dilution with the steel, can significantly change the resulting microstructure in the fusion zone.

Several experimental studies have been conducted to investigate the behavior of the solidification in superalloys containing Nb [5–10]. DuPont and Robino [11] reported that these alloys generally solidify through a three step process, which includes: (1) primary solidification $L \rightarrow \gamma$, followed by (2) a reaction in the eutectic type $L \rightarrow (\gamma + NbC)$, which occurs over a broad temperature range, followed by (3) a reaction of the eutectic terminal $L \rightarrow (\gamma + Laves)$ that occurs over a range with smaller final temperature.

Recent studies have also reported the presence of precipitates that are rich in C, N, Nb and Ti for the microstructure of dissimilar welding alloys 625 [12,13], whose presence can alter the solidification behavior of these alloys furthermore. Knowing the microchemical and microstructural evolutions during the solidification of these stated alloys is essential for the understanding of the relationship between the metallurgical aspects and the properties of these alloys. This research presents a new insight on the path in the solidification of 625 superalloy weld metals deposited by the TIG cold wire feed process on the C–Mn steel plates.

2. Experimental procedure

The welds were made through the TIG process with a cold wire automatic feeding system. The deposition was in a flat position. Multiple weld beads were deposited side by side, in order to produce a coating layer. The wire filler metal was the AWS ER NiCrMo-3, similar to the alloy Inconel® 625. The base metal is the ASTM A516 Gr.60 steel. Both chemical compositions are shown in Table 1. The shielding gas was pure argon.

The welding parameters used were the following: welding current ranging from 285 A to 335 A; the welding voltage 20–24 V; welding speed 17–25 cm/min; welding energy 10–16 kJ/cm; feed rate wire 6–9 m/min; distance from the tip of the electrode to the workpiece with a constant 10 mm; flow of shielding gas with 15 L/min and tecimento in three different types of motion (spiral, double-8, triangular).

After the welding, samples from the coatings were extracted and being conventionally prepared for a metallographic analysis. The microstructures were examined by a scanning electron microscope (SEM) models Phillips XL30 and Carl Zeiss EVO 40, both equipped with energy dispersive X-ray spectroscopy (EDS) systems. Samples for characterization by the transmission electron microscopy (TEM) were produced and analyzed using a JEOL JEM 2100 ARP microscope coupled with the EDS microanalysis system.

3. Results

The chemical composition of the weld metal volume, indicated a strong segregation of elements such as Mo and Nb to the interdendritic region, whereas elements such as Ni, Cr and Fe showed a slight depletion in these regions (interdendritic), as shown in Fig. 1.

The chemical composition profile crossing some of the dendrites in the transverse direction in relation to the direction of solidification (Fig. 2), clearly shows the variation of the elements. A significant increase in the Ni content and a slight rise of the Fe and Cr in the region of the dendrite nucleus has been observed. For the interdendritic regions identified in Fig. 2 by arrows, it can be observed an increase in the levels of Mo and Nb.

The distribution coefficient (k) denotes the intensity and direction of a microsegregation expected for a given element, during the solidification of an alloy $k = C_s/C_0$. Table 2 shows the concentrations of the dendrite center (C_s) and the interdendritic region (C_i), as well as the nominal composition (C_0) and the distribution coefficient (k) for two samples welded with the alloy 625, having been welded with a low heat input (T1) and the other welded with a higher heat input (T4). Considering a normal solidification process commonly encountered in the arc welding, the region in the center of the dendrite is the first region to solidify, and should present a kC_0 concentration, where C_0 is the nominal composition of the alloy (weld metal considering the dilution with the substrate). Based on the composition of the solid (C_s) shown in Table 2 and the nominal composition of the alloy (C_0) determined experimentally by XRF, the values of k for each element were calculated and presented in Table 2. The C_s values are also given in Table 2.

It has been found that the k coefficient of elements such as Ni and Fe (Table 2), had values slightly higher than 1, indicating a slight segregation of these elements into the solid. As for Cr, the values were also higher than 1, therefore its behavior resembles the following elements, Fe and Ni. The Mo already had a distribution coefficient of less than 1,

Table 2 – Chemical composition in the dendrite nucleus (C_s), in interdendritic region (C_i) and the global chemical composition (C_0), as well as the partitioning coefficient k.

Element	Sample T1				Sample T4			
	C_s	C_i	C_0	K	C_s	C_i	C_0	K
Ni	60.1 ± 2.9	52.6 ± 1.5	58.5	1.03	62.2 ± 2.2	58.6 ± 1.3	60.1	1.04
Cr	21.6 ± 0.7	19.6 ± 0.8	21.1	1.02	21.2 ± 1.2	20.7 ± 1.4	20.5	1.04
Mo	7.7 ± 1.5	12.3 ± 1.2	8.1	0.95	7.9 ± 1.5	10.1 ± 1.9	8.9	0.89
Nb	1.6 ± 0.9	6.5 ± 2.0	3.2	0.50	1.5 ± 0.4	6.2 ± 1.0	3.1	0.49
Fe	8.8 ± 1.0	8.9 ± 0.8	8.0	1.09	7.1 ± 0.9	7.0 ± 0.5	6.2	1.14

segregating to the liquid metal and enriching the interdendritic region in the end stage of solidification. Like Mo, Nb also segregates to the liquid, however with a greater intensity when compared to the Mo. Therefore, this strong segregation of the Nb has been appointed as primarily responsible for the formation of the secondary phases observed in the microstructure of the coatings in the alloy 625.

In fact, concerning alloys containing some quantities of Nb added, such as the 625 alloy, it has been observed that there is a characteristic profile of segregation, as shown in Fig. 2. Cieslak et al. [5] determined the distribution of chemical elements along the dendrites through an microprobe analysis, checking that elements such as Nb, Mo, Ti and Si ($k<1$), segregate significantly to the interdendritic region, while the centers of dendrites become depleted of these said elements and rich in Ni and Fe ($k>1$), since the Cr was not seen as an evidence of this segregation element to the interdendritic region. Furthermore, a similar behavior was duly observed by DuPont et al.

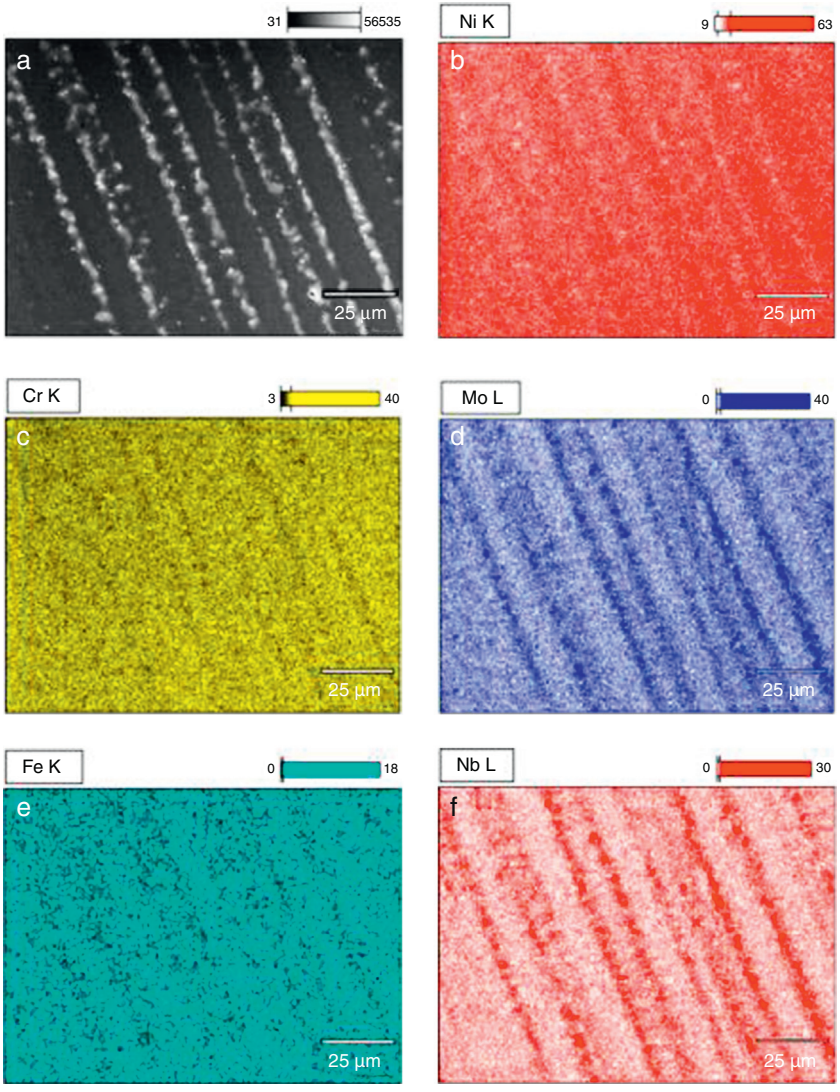

Fig. 1 – Elemental chemical mapping obtained by scanning electron microscope/energy dispersive X-ray spectroscopy of the bulk of weld metal indicating the strong segregation of Mo and Nb from the dendritic nucleus to interdendritic region.

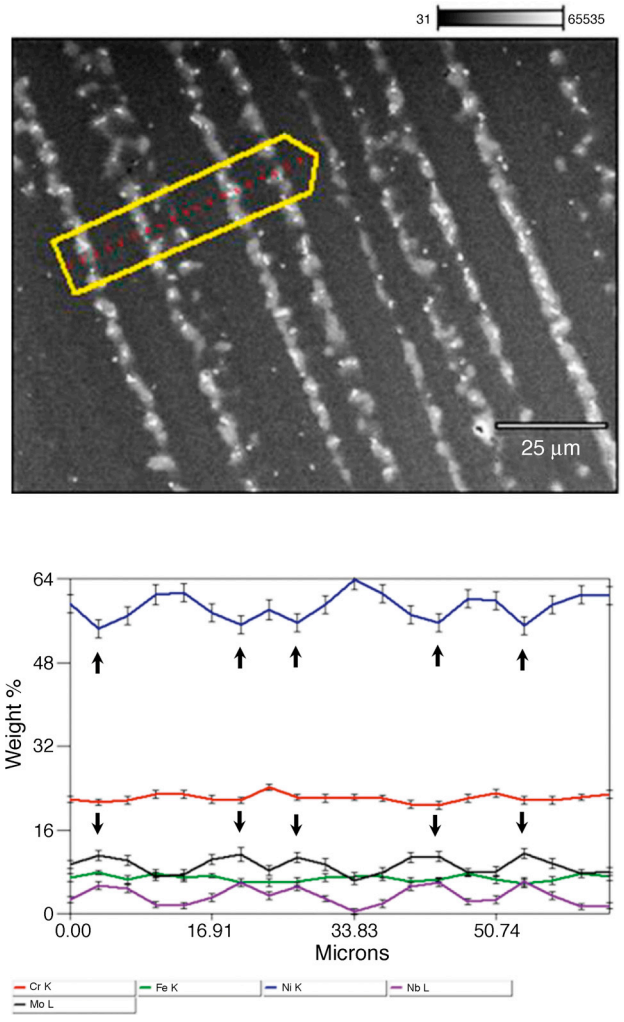

Fig. 2 – Elemental chemical profile crossing the dendrites and showing clearly the elemental segregation during the solidification process. The arrows indicate the interdendritic region.

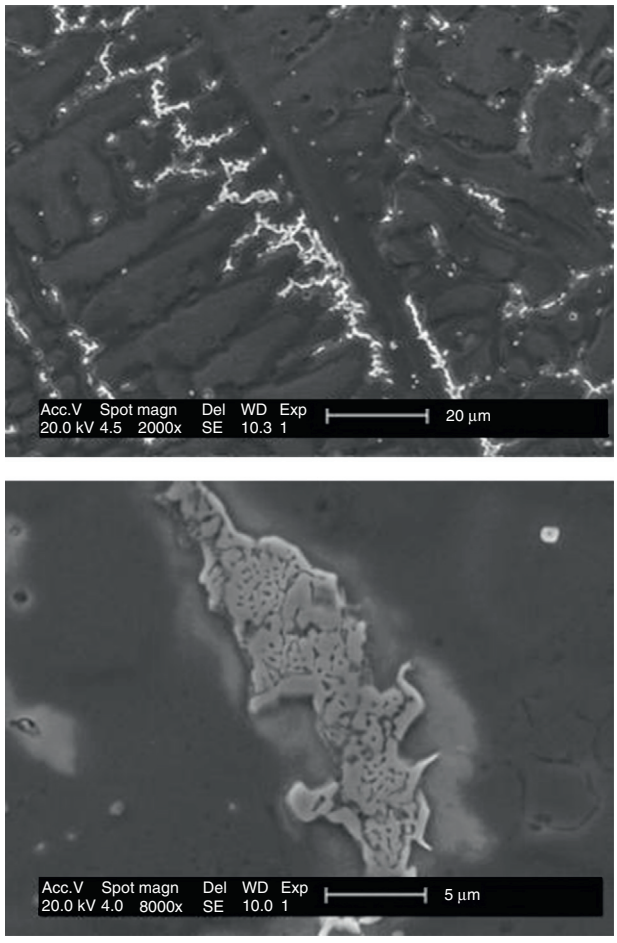

Fig. 3 – (a) Secondary phases formed along the interdendritic region. (b) Enlarged image showing the eutectic morphology of the said phase.

[14]. The results observed in this study are also consistent with the profile of segregation shown by other authors [15,16].

Regarding the microstructural characterization, metallographic analyzes were performed by SEM and the results indicated the presence of two main types of secondary phases. The first type of secondary phase commonly observed in the microstructure of the fusion zone, was typically found along the intercellular or interdendritic regions. As seen in Fig. 3, this precipitation exhibits a eutectic morphology, which is also observed in the elongated form or rod-shaped.

The chemical mapping by EDS in some of these phases, indicated an enrichment of Mo and Nb, as well as the presence of Si at higher concentrations (Fig. 4). With reference to the elements Ni, Fe and Cr, a depletion region in the secondary phase has been observed. Based on the chemical composition and morphology, such particles were characterized as Laves phase rich in Nb. These results are consistent with those reported by other authors evaluating the microstructure of the alloy 625 [15–17].

Using the transmission electron microscopy, some of aforesaid particles with elongated morphology and high concentrations of Nb, were correctly identified by the selected area electron diffraction (SAD). Fig. 5 shows an image obtained through the TEM bright field mode in such rod-shaped particles is identified as Nb rich Laves phase. The electron diffraction pattern (SADP) is oriented in the axis of the zone [322] = [4156].

Unlike what is commonly observed for the alloy Inconel 625 weld metal, an additional type of secondary phase with a cuboidal morphology was identified in this study, as shown in Fig. 6. The presence of this type of precipitate has not been reported for the alloy 625 in the literature. A preliminary analysis by the SEM/EDS indicated that these cubic particles are rich in Nb, Ti, C and N, aside from the references pointed out in the first case as a particular type of carbonitride of Ti and Nb.

Another observation that is rarely reported in the literature, is regarding the presence of titanium in particles precipitated. Countless studies on the microstructure of the alloy 625, have been reported in the literature, however, only a few papers did mention the occurrence of carbides or carbonitrides containing Ti. As a general rule, these carbides

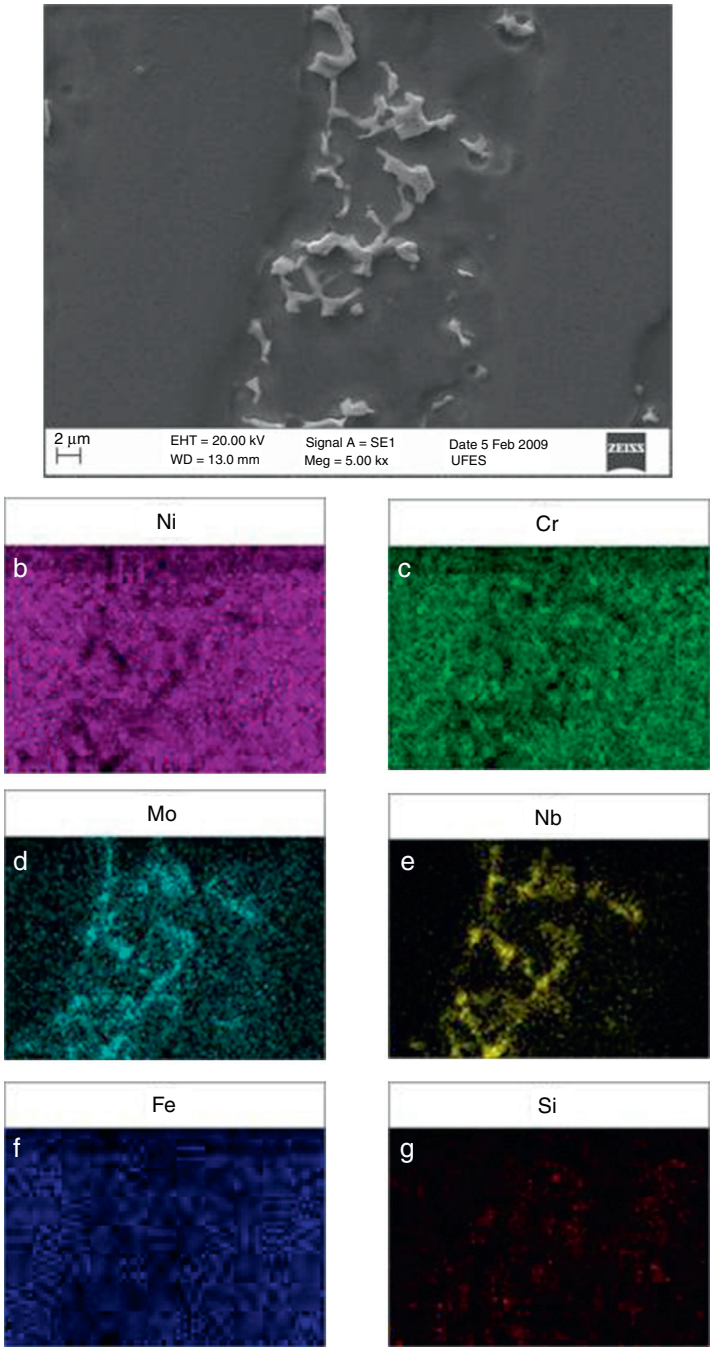

Fig. 4 – (a) Scanning electron microscopy micrograph obtained in scanning electron operation mode showing the γ matrix and the eutectic secondary phase. The elemental chemical maps obtained by energy dispersive X-ray spectroscopy: (b) Ni; (c) Cr; (d) Mo; (e) Nb; (f) Fe; (g) Si.

were characterized as NbC, being both case for materials heat treated and aged [18,19], as well as in welded conditions [5,20].

TEM analysis was performed and showed that some precipitates cubic looks as similar to a combination of a particle within another. An example of this complex particle is shown in Fig. 7. It is possible to identify an initial particle with planar facets inside the precipitate, surrounded by a shell in this particular image. The overall particle was identified by selected area electron diffraction (SAD), as a primary carbide NbC type. However, the chemical EDS mapping showed a strong partition of Ti, N and Nb, as can be seen in Fig. 7. The presence of large concentrations of Ti and N in the interior of the precipitate, shows that there is a particle of titanium nitride (TiN) forming the core of the said precipitate. The map of the Nb shows a depletion of this element to the center of the particle and a high concentration of it along the edge of the precipitate, forming a Nb-rich shell around the core, which is rich in Ti and N. The carbon in turn, at first did not show any preferential distribution.

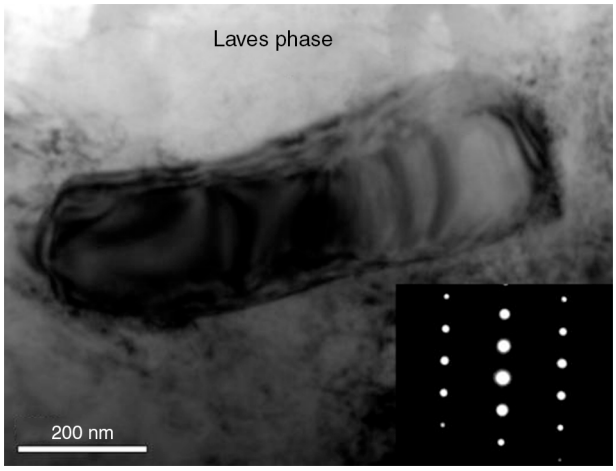

Fig. 5 – (a) Transmission electron microscopy image in bright field of a rod-shaped Laves phase and its respective selected area electron diffraction pattern on [322] = [4156] zone axis.

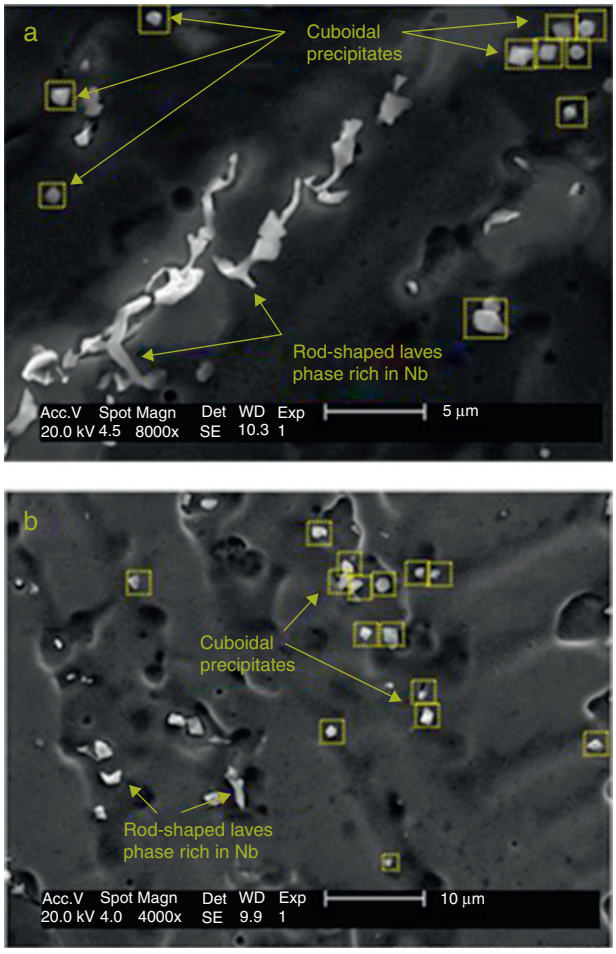

Fig. 6 – Scanning electron microscope micrograph showing the main morphologies of secondary phases observed into the weld metal.

Therefore, the cubic precipitates rich in Nb and Ti present in the weld metal are not a simply carbonitrides, but the combination of a titanium nitride core (TiN) surrounded by a niobium carbide shell (NbC and/or NbTiC). This hypothesis is supported by experimental results. However, there were significant variations in chemical composition within the cubic precipitates and no significant change was found in a crystallographic form. In fact, changes in the crystallographic features of the precipitate are unlikely, since both have a cubic crystal structure (NaCl) and very similar lattice parameters: TiC (0.4327 nm) [21], TiN (0.4235 nm) [22], Ti(CN) (0.4297 nm) [23], NbC (0.4449 nm) [24], and (NbTi)C (0.4427 nm) [25].

These stated results indicated that a complex precipitation mechanism may occur during the welding of these said alloys, depending in the chemical composition of the weld metal. The high melting point of the TiN nitrides (2927 °C) [25], which is approximately twice the *liquidus* temperature of the 625 alloy, therefore, allowing them to remain in the solid state within the volume of the liquid pool. This makes them excellent nucleating agents for the formation of Nb carbides, as well as providing a good surface for nucleation possessing crystallographic and chemical affinities.

Fig. 8 shows another form of precipitation found in the present study, in which a nitride TiN core leads to a structure called NbC arms. Indeed, various precipitates were observed in the form of Nb-rich arms or needles, growing from a central core of TiN. Observing the chemical mapping obtained by the EDS, it is clearly noted that a strong concentration of Ti is only at the apex of the V structure formed by the TiN core and the NbC arms. The Nb is particularly enriched in the V structure.

4. Discussion

As it has been seen, dilution greatly influences the microstructure in the resulting alloy during solidification. Two important elements being C and Si, strongly influence the formation of the carbide and the Laves phase, respectively. Evaluating the binary Ni–Nb diagram obtained by Thermocalc® (Fig. 9), shows that there is no formation of this phase in this binary system, requiring the presence of other elements in their favor. In this context, Fe also becomes a very important element to favor the formation of the Laves phase in Ni alloys, given their ability to form the Laves phase type Fe_2Nb.

DuPont [20] studied the process of solidification for the alloy 625 welded with a 2.25 Cr–1Mo steel substrate and verified the actual role of the Fe in the weld overlay of these alloys. This particular author reports that the significant Fe enrichment of the alloy 625, due to the dilution with the substrate, was preponderant to the microstructure resultant from solidification, which occurred over a temperature range of 170 °C, in the following sequence:

$$L \rightarrow L + \gamma \rightarrow L + \gamma + \text{Laves} \rightarrow \gamma + \text{Laves}$$

Another factor mentioned by DuPont [20] for this route of solidification, was the low C content in the substrate, which was 0.13 wt.%. Considering the C content in the substrate used in this study, C = 0.15% (ASTM A516 Gr.60), it resembles the C content of the substrate used by DuPont [20]. Zhao et al. [9] studied the microstructure of the alloy 625 filler metal welded

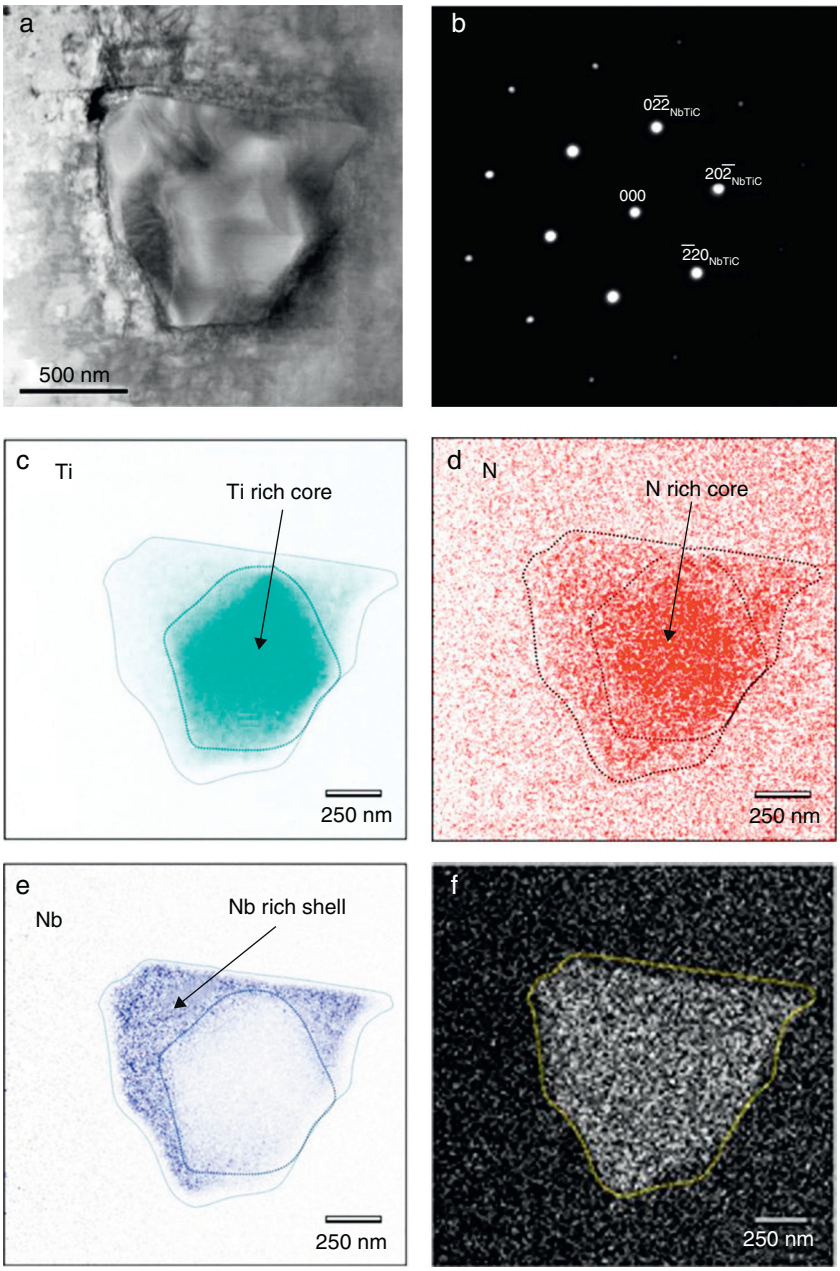

Fig. 7 – (a) Transmission electron microscopy image in bright field showing a core/shell complex precipitate. (b) Selected area electron diffraction pattern on [1 1 1] zone axis. Elemental chemical mapping by energy dispersive X-ray spectroscopy: (c) Ti; (d) N; (e) Nb; (f) C.

with carbon steel in a content of 0.25 wt.% and observed the presence of both phases, Nb-rich carbide and Nb-rich Laves phase, however, the carbon content in the substrate is 40% higher than the ASTM A516 Gr.60.

Cieslak et al. [5] studied the solidification of the alloy 625 with varying levels of C, Si and Nb. These authors found that when the alloy contained low amounts of C (0.009 wt.%) and Si (0.03 wt.%), together with a Fe content of 2.3 wt.%, as well as 3.6 wt.% of Nb, there was a small volume fraction of secondary interdendritic phase (0.3% vol.) consisting of the Nb-rich Laves phase and MC carbides (NbC). However, when there was an addition of 0.038 wt.% C, occurring only the formation of MC carbides (NbC), thus, indicating that the presence of C, even in a small amount, may still have been able to suppress the formation of the Laves phase. In another alloy, which was added with 0.38 wt.% Si and a low carbon content, there was a formation of the Laves phase rich in Nb and M_6C type carbides. When C (0.035 wt.%) was added together with Si (0.46 wt.%), the following two phases were formed during solidification: MC carbide (NbC) and Nb-rich Laves phase. All these said results were confirmed by a differential thermal analysis and by electron microscopy.

Theoretically, only considering the similarities between the C content of the substrates used in this study and also used by

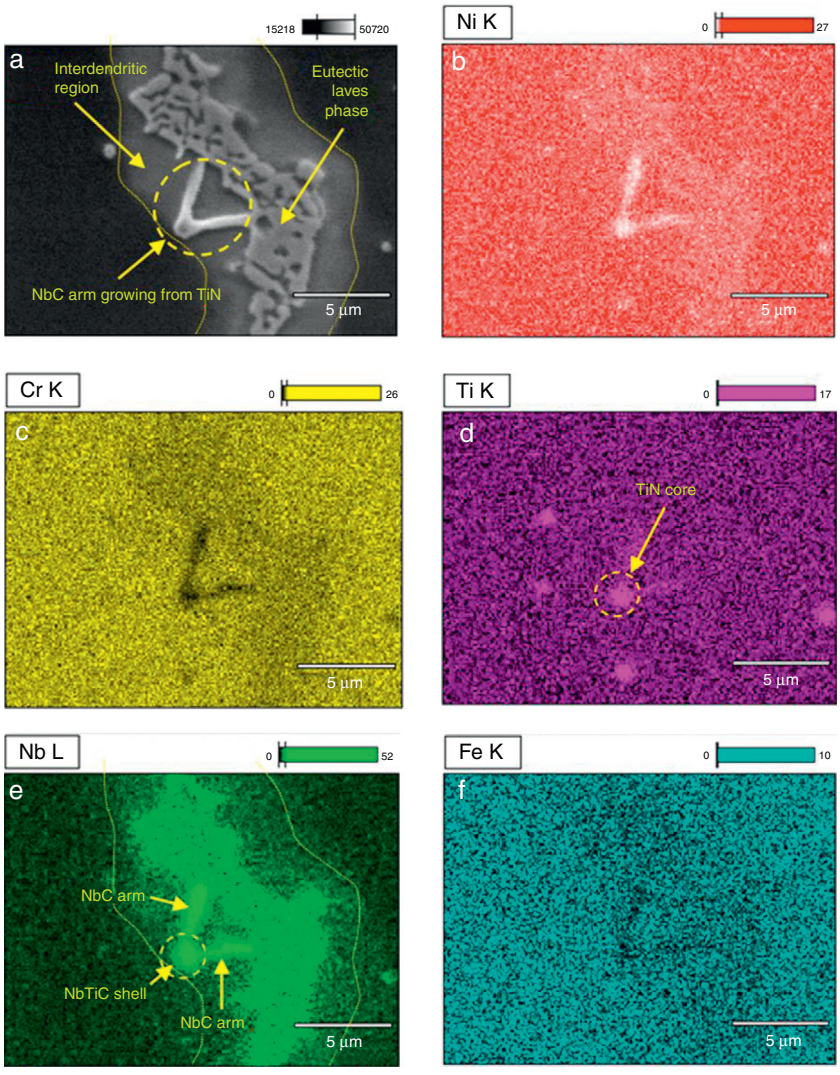

Fig. 8 – (a) Scanning electron microscope micrograph indicating the presence of a eutectic Laves phase and a V-shaped complex precipitate. The elemental chemical mapping obtained by energy dispersive X-ray spectroscopy: (b) Ni; (c) Cr; (d) Ti; (e) Nb; (f) Fe.

DuPont [20], one would be expected that the end of the solidification occurred only in the formation of the eutectics Nb-rich Laves phase. However, the Fe contents in the weld overlays due to the dilution with the substrate, ranging between 6 and 15%. These particular values are well below to the Fe content recorded by DuPont [20] for alloy 625 with a Fe content of 28 wt%, being the solidification enough to form only Laves phase as secondary constituent.

Therefore, it is possible that lower levels of Fe in the coatings studied herein, are sufficient to enable a complete solidification of the interdendritic liquid (rich in Nb) Laves phase. In fact, DuPont [20] has noted that increasing the Fe content in the alloy 625, seemed to favor the formation of the Laves phase rich in Nb, to the point of completely suppressing the formation of NbC carbides. It is worthwhile noting that the study of the DuPont [20] the overlay was deposited under a single condition of welding parameters, however, not being assessed the effects of factors other than the chemical composition.

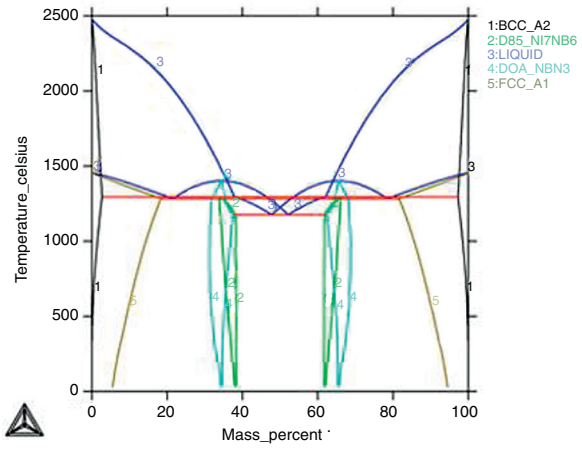

Fig. 9 – Binary phase diagram for the system Ni-Nb calculated with ThermoCalc.

In addition, it ought to be highlighted the important role of titanium nitride TiN present in the weld metal, whose high melting point makes them excellent nucleating agents for the formation of niobium and titanium carbides shells (NbTi)C and NbC carbides arms, during the solidification of the alloy. Another important information is that the solidification temperature of the carbide NbC (~1325 °C) is higher than the one of the Nb-rich Laves phase (~1266 °C), making their favorable nucleation and growth before the Laves, which explains the formation of the shells and the arms of carbides, during solidification, as seen in Figs. 7 and 8. In fact, a new route to explain the solidification process of the alloy 625, is proposed in this study, as shown below:

$$L + (\mathrm{TiN}) \rightarrow L + \gamma + (\mathrm{TiN}) \rightarrow L + \gamma + (\mathrm{TiN}) + (\mathrm{NbTi})\mathrm{C}\,[\mathrm{shell}]$$
$$\rightarrow L + \gamma + (\mathrm{TiN}) + (\mathrm{NbTi})\mathrm{C}[\mathrm{shell}] + \mathrm{Laves}$$
$$\rightarrow \gamma + (\mathrm{TiN})[\mathrm{core}]/(\mathrm{NbTi})\mathrm{C}[\mathrm{shell}] + \mathrm{Laves}$$

Or considering the growth of NbC arm from the NbTiC shell, the complete solidification path to be considered is:

$$L + (\mathrm{TiN}) \rightarrow L + \gamma + (\mathrm{TiN}) \rightarrow L + \gamma + (\mathrm{TiN}) + (\mathrm{NbTi})\mathrm{C}\,[\mathrm{shell}]$$
$$\rightarrow L + \gamma + (\mathrm{TiN}) + (\mathrm{NbTi})\mathrm{C}[\mathrm{shell}] + \mathrm{NbC}[\mathrm{arm}]$$
$$\rightarrow L + \gamma + (\mathrm{TiN}) + (\mathrm{NbTi})\mathrm{C}[\mathrm{shell}] + \mathrm{NbC}[\mathrm{arm}] + \mathrm{Laves}$$
$$\rightarrow \gamma + (\mathrm{TiN})[\mathrm{core}]/(\mathrm{NbTi})\mathrm{C}[\mathrm{shell}]/\mathrm{NbC}[\mathrm{arm}] + \mathrm{Laves}$$

Initially, there was a weld pool volume completely in liquid state with the presence of solid particles of titanium nitride (TiN). With the onset of the solidification occurring γ phase formation, segregating elements such as Nb, Ti, Mo and Si to the interdendritic liquid and gradually pushing TiN particles in the liquid, a subsequent growth began with the shell forming of Nb and Ti carbides (NbTi)C on the surface of the titanium nitride (TiN) preexisting. Depending upon the welding conditions and consequently the solidification rate, these stated complex precipitates of nitride/carbide may be entrapped by the solid and are retained near the center of the dendrite. However, if the solidification rate is favorable to the precipitation, it may occur the growth of niobium carbide arms (NbC). With the continued solidification process occurring, a significant increase of Nb concentration in the interdendritic liquid would cause the formation of the Laves phase rich in Nb. As an end result, a microstructure consisting of a matrix γ, the complex precipitate (TiN) [core]/(NbTi)C [shell] and/or NbC [arm] carbides, as well as the Nb-rich Laves phase.

5. Conclusions

Based on the results presented with this study, the microstructure of the nickel-based superalloy weld overlays deposited with type Inconel 625 by TIG cold wire feed welding process, concludes the following facts:

- The Nb microsegregation during solidification significantly influences the behavior of the alloy solidification.
- Cubic precipitates observed in the microstructure, showed characterized as a complex precipitate, consisting of a core with titanium nitride (TiN) surrounded by a niobium titanium carbide (NbTi)C.
- Due to the Nb microsegregation to an interdendritic volume during the solidification, there was a formation of the eutectic Laves phase, rich in Nb.
- Depending on the microstructural characteristics duly observed, we hereby propose a new solidification path to the alloy Inconel 625:

$$L + (\mathrm{TiN}) \rightarrow L + \gamma + (\mathrm{TiN}) \rightarrow L + \gamma + (\mathrm{TiN}) + (\mathrm{NbTi})\mathrm{C}[\mathrm{shell}]$$
$$\rightarrow L + \gamma + (\mathrm{TiN}) + (\mathrm{NbTi})\mathrm{C}[\mathrm{shell}] + \mathrm{Laves}$$
$$\rightarrow \gamma + (\mathrm{TiN})[\mathrm{core}]/(\mathrm{NbTi})\mathrm{C}[\mathrm{shell}] + \mathrm{Laves}$$

- Considering the growth of NbC arm from the NbTiC shell, the complete solidification path to be considered is:

$$\mathrm{L} + (\mathrm{TiN}) \rightarrow \mathrm{L} + \gamma + (\mathrm{TiN})$$
$$\rightarrow \mathrm{L} + \gamma + (\mathrm{TiN}) + (\mathrm{NbTi})\mathrm{C}[\mathrm{shell}]$$
$$\rightarrow \mathrm{L} + \gamma + (\mathrm{TiN}) + (\mathrm{NbTi})\mathrm{C}[\mathrm{shell}] + \mathrm{NbC}[\mathrm{arm}]$$
$$\rightarrow \mathrm{L} + \gamma + (\mathrm{TiN}) + (\mathrm{NbTi})\mathrm{C}[\mathrm{shell}] + \mathrm{NbC}[\mathrm{arm}] + \mathrm{Laves}$$
$$\rightarrow \gamma + (\mathrm{TiN})[\mathrm{core}]/(\mathrm{NbTi})\mathrm{C}[\mathrm{shell}]/\mathrm{NbC}[\mathrm{arm}] + \mathrm{Laves}$$

Conflicts of interest

The authors declare no conflicts of interest.

Acknowledgements

The authors would like to thank the PETROBRAS for providing the support for this research and our colleagues in the Welding Engineering Laboratory at Universidade Federal do Ceará (Federal University of Ceará), especially Professor Willys M. Aguiar for the insightful discussion. Also grateful the Brazilian Synchrotron Light Laboratory (LNLS) and Brazilian Center of Nanoscience and Nanotechnology (C2Nano) for their support in TEM analysis using Jeol JEM 2100 HTP microscope. They are also grateful to Brazilian research agencies (CNPq, CAPES and FINEP) for financial support.

REFERENCES

[1] Perepezko JH. The hotter the engine, the better. Science 2009;326:1068–9.
[2] Sims CT, Stoloff NS, Hagel WC. Superalloys II. New York: John Wiley & Sons; 1987.
[3] Hodge FG. History of solid-solution-strengthened Ni alloys for aqueous corrosion service. JOMMER 2006;58:28–31.
[4] Silva CC, Afonso CRM, Ramirez AJ, Motta MF, Miranda HC, Farias JP. Metallurgical aspects of dissimilar weld overlays of

inconel 625 nickel based superalloys. [In Portuguese]. Soldagem & Inspeção 2012;17:251–63.
[5] Cieslak MJ, Headley TJ, Kollie T, Romig AD. A melting and solidification study of alloy 625. Metall Trans A 1988;19A:2319–31.
[6] Knorovsky GA, Cieslak MJ, Headley TJ, Romig AD, Hammetter WF. INCONEL 718: a solidification diagram. Metall Trans A 1989;20:2149–58.
[7] Nakao Y, Ohshige H, Koga S, Nishihara H, Sugitani J. Effect of Nb/C on the sensitivity of liquation cracking in 24Cr-24Ni-1. SNbFe-base heat resisting alloy. J Jpn Weld Soc 1982;51:989–95.
[8] Radhakrishnan B, Thompson RG. Solidification of the nickel-base superalloy 718: a phase diagram approach. Metall Mater Trans A 1989;20:2866–8.
[9] Zhao QH, Gau YP, Devletian JH, McCarthy JM, Wood WE. Microstructural analysis of Ni alloy 625 cladding over carbon steel. In: Proceedings of 3rd International Conference on Trends in Welding Research. Materials Park, OH: ASM International; 1993. p. 339–43.
[10] DuPont JN, Robino CV, Marder AR, Notis MR. Solidification of Nb-bearing superalloys: part II. Pseudoternary solidification surfaces. Metall Mater Trans A 1998;29A:2797–806.
[11] DuPont JN, Robino CV. The influence of Nb and C on the solidification Microstructures of Fe–Ni–Cr alloys. Scripta Mater 1999;41:449–54.
[12] Silva CC, Afonso CRM, Miranda HC, Ramirez AJ, Farias JP. Microstructure of alloy 625 weld overlay. In: AWS Fabtech Conference. 2011.
[13] Silva CC, Miranda HC, Farias JP, Afonso CRM, Ramirez AJ. Carbide/nitride complex precipitation – an evaluation by analytical electron microscopy. In: 17th international microscopy congress. 2010.
[14] DuPont JN, Banovic SW, Marder AR. Microstructural evolution and weldability of dissimilar welds between a super austenitic stainless steel and nickel-based alloys. Weld J 2003;82:125–56.
[15] Banovic SW, DuPont JN, Marder AR. Dilution and microsegregation in dissimilar metal welds between super austenitic stainless steel and nickel base alloys. Sci Technol Weld Joining 2002;7:374–83.
[16] Cieslak MJ, Headley TJ, Knorovsky GA, Romig Jr AD, Kollie T. A comparison of the solidification behavior of INCOLOY 909 and INCONEL 718. Metall Trans A 1990;21A:479–88.
[17] DuPont JN, Robino CV, Michael JR, Notis MR, Marder AR. Solidification of Nb-bearing superalloys: part I. Reaction sequences. Metall Mater Trans A 1998;29A:2785–96.
[18] Mathew MD, Parameswaran P, Rao KBS. Microstructural changes in alloy 625 during high temperature creep. Mater Charact 2008;59:508–13.
[19] Shankar V, Rao KBS, Mannan SL. Microstructure and mechanical properties of Inconel 625 superalloy. J Nucl Mater 2001;288:222–32.
[20] DuPont JN. Solidification of an alloy 625 weld overlay. Metall Mater Trans A 1996;27A:3612–20.
[21] Powder Diffraction File. Swarthmore, PA: International Center for Diffraction Data; 1987.
[22] Guilemany JM, Sanchiz I, Alcobé X. X-ray diffraction analysis of titanium carbonitride 30/70 and 70/30 solid solutions. Powder Diffr 1992;7:34–5.
[23] Goldschmidt HJ. Interplanar spacings of carbides in steels. Metallurgia 1949;40:103–4.
[24] Morra M, Ballinger R, Hwang I. Incoloy 908, a low coefficient of expansion alloy for high strength cryogenic applications – Part I. Physical metallurgy. Metall Trans A 1992;23: 3177–92.
[25] Lengauer W. Transition metal carbides, nitrides and carbonitrides. In: Riedel R, editor. Handbook of ceramic hard materials, vol. 1. Weinheim: Wiley–VCH; 2000. p. 202–52.